A Study of Motion Artifacts of Fourier-Based Image Construction

Jing Wang and Jian-yu Lu, Department of Bioengineering, The University of Toledo, Toledo, OH 43606, USA, jilu@eng.utoledo.edu

***Abstract* — Based on the high frame rate imaging method developed in our lab, a Fourier-based imaging method with a variable frame rate was developed recently. In this method, multiple steered plane waves or limited diffraction beams are transmitted to obtain ultrasound echo signals. Images are constructed with Fourier transformations. Because multiple transmissions may be used to obtain a frame of image to increase image resolution, field of view, and to reduce sidelobe, it is important to study the effects of motion on the method for fast moving objects such as the mitral valve of the heart, and compare the results with those obtained with the conventional delay-and-sum method. In this paper, *in vitro* experiments with a point scatterer and a tissue-mimicking phantom are performed. Image resolution, sidelobe, and contrast are obtained for both moving and stationary objects. Results show that the Fourier-based imaging method is not sensitive to the motion except when the number of transmissions is large (lower frame rate) and the depth is small.**

Keywords- Motion artifacts; High frame rate imaging; Medical imaging; Fourier; Limited diffraction beams.

I. INTRODUCTION

Based on limited diffraction beam theory [1]-[3], a high frame rate (HFR) imaging method was developed in 1997 [4]-[6]. In this method, only one plane wave transmission is needed to construct a frame of two-dimensional (2D) or three-dimensional (3D) ultrasound image at a frame rate up to 3750 frames/s for biological soft tissues at a depth of 200 mm. The ultrahigh frame rate is useful for imaging fast moving objects such as mitral valve of the heart and getting blood flow vector images. In addition, because fast Fourier transform (FFT) and inverse fast Fourier transform (IFFT) are used in image reconstruction, hardware can be greatly simplified due to reduced computations, especially, in 3D imaging.

Although the HFR imaging method has some advantages, its sidelobe is relatively high due to a lack of transmission focusing. In addition, image field of view is relatively small (same as the transducer aperture). To reduce sidelobe and increase field of view and image resolution, the HFR imaging theory was extended recently to include multiple steered plane waves or limited diffraction beams in transmission [7]-[8]. In addition, it was proved that limited diffraction beam weighting on a receive aperture is exactly the same as the Fourier transform over the same aperture [8]. The extended HFR method allows a continuous compromise between image quality and frame rate. This is desirable in applications where high frame rate imaging is not crucial, such as imaging of livers or kidneys, high quality images can be reconstructed at the expense of image frame rate.

This work was supported in part by a grant, HL60301, from the National Institute of Health of USA.

Because the extended HFR imaging method may use multiple transmissions to obtain a frame of image, it is important to study the motion artifact of the method. In this paper, *in vitro* experiments are performed with the extended HFR imaging method at various frame rates. Results are compared with those obtained with the conventional delay-and-sum (D&S) method with a fixed transmission focus and dynamic reception focusing, as well as with the D&S method with dynamic focusing in both transmission and reception (dynamic transmission focusing is achieved using montage process that may reduce image frame rate dramatically).

II. FORMULAE FOR IMAGE RECONSTRUCTION

From X waves [1]- [3], one obtains limited diffraction array beams [9] for both transmission and reception. Following the derivations of HFR imaging (Equation (1)-(15) of [4], [5], Equations (1)-(11) of [8]), one obtains a relationship between the Fourier transform ($\tilde{R}_{k_x+k_{x_T},k_y+k_{y_T},k_z+k_{z_T}}(\omega)$) of received echo signals in terms of both time (t) and transducer aperture (or limited diffraction reception aperture weighting) and a 3D spatial Fourier transform of the object function [7]-[8]:

$$\tilde{R}_{k_x+k_{x_T},k_y+k_{y_T},k_z+k_{z_T}}(\omega)=\frac{A(k)T(k)H(k)}{c^2}\times F(k_x+k_{x_T},k_y+k_{y_T},k_z+k_{z_T}), \quad (1)$$

or

$$F_{BL}(k_x^{'},k_y^{'},k_z^{'})=c^2H(k)\tilde{R}_{k_x^{'},k_y^{'},k_z^{'}}(\omega)$$

where $A(k)$ and $T(k)$ are transmission and reception transfer functions, respectively, $H(k)$ is the Heaviside step function [10], $\vec{K}^T=(k_{x_T},k_{y_T},k_{z_T})$ and $\vec{K}^R=(k_x,k_y,k_z)$ are transmission and reception wave vectors, respectively, $F(\cdot)$ is the Fourier transform of the object function, $f(\vec{r}_0)$, where $\vec{r}_0=(x_0,y_0,z_0)$ is a point in space, $F_{BL}(\cdot)=A(k)T(k)F(\cdot)$ is a band-limited version of $F(\cdot)$ ($H(k)$ is moved to the side of $\tilde{R}(\cdot)$ for convenience), $k=\omega/c$ is the wave number, where ω is the angular frequency and c is the speed of sound, and where

$$\begin{cases} k_x^{'}=k_x+k_{x_T} \\ k_y^{'}=k_y+k_{y_T} \\ k_z^{'}=k_z+k_{z_T}=\sqrt{k^2-k_x^2-k_y^2}+\sqrt{k^2-k_{x_T}^2-k_{y_T}^2}\geq 0 \end{cases}. \quad (2)$$

If $\vec{K}^T = (k_{x_T}, k_{y_T}, k_{z_T})$ is fixed for a wideband signal in each transmission, a limited diffraction array beam is transmitted. $\vec{K}^T$ can also be expressed in spherical coordinates:

$$\begin{cases} k_{x_T} = k \sin\zeta_T \cos\theta_T = k_{1_T} \cos\theta_T \\ k_{y_T} = k \sin\zeta_T \sin\theta_T = k_{1_T} \sin\theta_T \\ k_{z_T} = k \cos\zeta_T = \sqrt{k^2 - k_{1_T}^2} \geq 0 \end{cases}, \quad (3)$$

where ζ_T is an Axicon (or steering) angle [1]-[2] of X wave, θ_T is a rotation angle of a transmission beam around the axial axis of the transducer, and $k_{1_T} = k \sin\zeta_T = \sqrt{k_{x_T}^2 + k_{y_T}^2}$. If the pair, (ζ_T, θ_T), is fixed, it means a plane wave is transmitted.

From (1), 3D images can be reconstructed with an inverse Fourier transform:

$$\begin{aligned} f(\vec{r}_0) &\approx f_{BL}(\vec{r}_0) \approx f_{BL}^{Part}(\vec{r}_0) \\ &= \frac{1}{(2\pi)^3} \int_{-\infty}^{\infty} dk_x' \int_{-\infty}^{\infty} dk_y' \int_{k \geq \sqrt{k_{xT}^2 + k_{yT}^2} \text{ and } k \geq \sqrt{k_x^2 + k_y^2}} dk_z' \cdot \quad (4) \\ &\times F_{BL}(k_x', k_y', k_z') e^{-ik_x' x_0 - ik_y' y_0 - ik_z' z_0} \end{aligned}$$

where the first approximation is due to the finite bandwidth of received signals and the second is due to the requirements that both $k \geq \sqrt{k_{x_T}^2 + k_{y_T}^2}$ and $k \geq \sqrt{k_x^2 + k_y^2}$ must be satisfied. To use FFT and IFFT for image reconstructions, mapping between the Fourier transform of received signals and the rectangular grid of the Fourier transform of the object function is required [7]-[8]. The mapping can be accomplished with a conventional interpolation method.

Equation (1) is also suitable for 2D imaging where k_{y_T} and k_y are set to zero [7]-[8]. In the following experiments, 1D array transducer is used for 2D image reconstructions. Furthermore, steered plane waves are assumed in transmissions.

III. EXPERIMENT

To study the effects of motion on the extended high frame rate imaging method [7]-[8], *in vitro* experiments are performed using the high frame rate imaging system [11]-[12] that we developed in house. Radio frequency (RF) data obtained are used to reconstruct images with the Fourier method [7]-[8] (see (1) above) and conventional D&S method.

A. Experiment with A Point Scatterer

In the experiment, a point scatterer is placed in the imaging plane, moving perpendicularly to the axis of a 2.5 MHz, 19.2 mm aperture, and 128 element broadband phased array transducer at a velocity of 214 mm/s that is higher than the peak velocity of the mitral valve of a normal human heart. Experiments are repeated with the point scatterer placed on the transducer axis at different depths (30, 46, 50, 70 and 90mm) from the transducer surface. At each depth, data from different numbers of transmissions (1, 11, 19, and 91) are used to reconstruct images with the Fourier method (at frame rates of 5346, 486, 281, and 59 frames/s, respectively).

As a comparison, images are also reconstructed with conventional delay-and-sum (D&S) method with and without dynamic focusing in transmission. (For D&S method without dynamic transmission focusing, the frame rate is about 59 frames/s. For D&S method with dynamic transmission focusing, the frame rate may be low although image quality may be high.)

B. Experiment with Ttissue Mimicking Phantom

To study the change of image contrast due to motion, an ATS539 tissue mimicking phantom is in place of the point scatterer with the center of its six 15mm diameter cylinders (-15 dB, -6 dB, -3 dB, +3 dB, +6 dB, and +15 dB relative to the background) located at a depth of 46 mm. The moving velocity the phantom is the same as that of the point scatterer.

IV. RESULTS

Line plots of point spread functions (PSFs) representing maximum sidelobe (along axial direction) at each transverse position for a stationary point scatterer are shown in Fig. 1. -6 dB resolution and the average sidelobe of each plot are listed in Table 1. It is seen from these results that the Fourier method with 91 transmissions has lower sidelobe and higher image resolution than the D&S method with either fixed or dynamic transmission focusing.

The percent changes of image resolution (R_c) and sidelobe (S_c) of a point scatterer due to motion are shown in Fig. 2. The definitions of the percent changes of resolution and sidelobe are given by

$$R_c = \frac{R_{moving} - R_{Stationary}}{R_{Stationary}} \times 100\% \quad (5)$$

and

$$S_c = \frac{S_{moving} - S_{Stationary}}{S_{Stationary}} \times 100\%, \quad (6)$$

respectively, where the subscripts "moving" and "stationary" represent the parameters obtained with and without motion, respectively.

Fig. 3 shows regions that are used for the calculation of contrasts of images with the following formula:

$$C = 20 \log \frac{\bar{m}_h}{\bar{m}_b}, \quad (7)$$

where $\bar{m}_h$ and $\bar{m}_b$ are mean values inside the envelope detected cylindrical object and the background, respectively.

Contrasts of cylindrical objects of a stationary ATS539 phantom are given in Table 2. They are correlated to the manufacturer-provided nominal contrasts of the phantom. The percent change of contrast due to motion of the ATS539 phantom is shown in Fig. 4. It is seen that the Fourier method with 91TXs has the highest percent change. The definition of

the percent change of contrast (C_c) is similar to those of image resolution and sidelobe:

$$C_c = \frac{C_{moving} - C_{Stationary}}{C_{Stationary}} \times 100\%, \quad (8)$$

where C_{moving} and $C_{Stationary}$ are contrast with and without motion of the phantom.

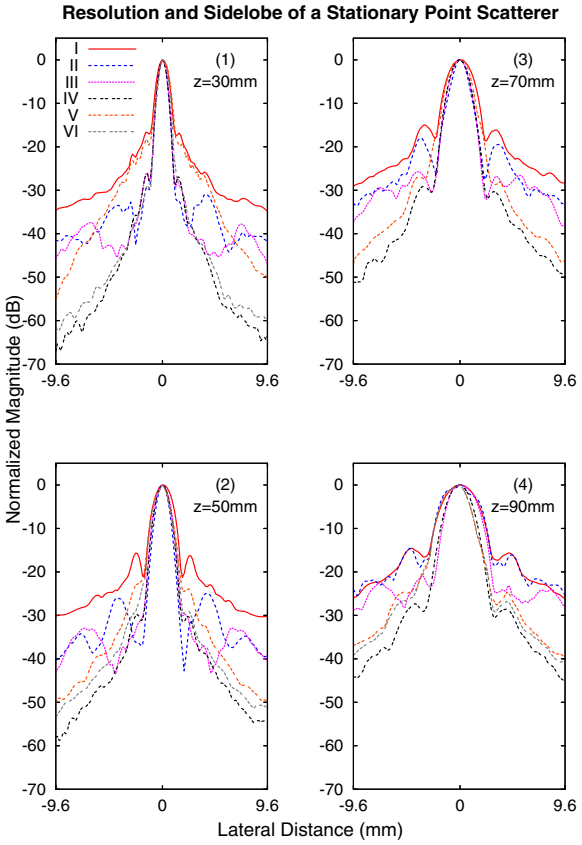

Figure 1. *In vitro* experiment with a stationary point scatterer located at depths of (1) 30, (2) 50, (3) 70, and (4) 90 mm, respectively, in water with a 2.5 MHz, 19.2 mm aperture, and 128 element broadband phased array transducer for different imaging methods. The line plots show the maximum envelope of the point spread functions (PSFs) of reconstructed images along the axial axis versus the transverse axis (in parallel with transducer surface) of the transducer. I – Fourier method with 1TX or 1 transmission (5346 frames/s); II – 11TXs or 11 transmissions (486 frame/s); III - 19 TXs or 19 transmissions (281 frame/s); IV - 91 TXs or 91 transmissions (59 frames/s); V – D&S or delay-and-sum method with a fixed transmission focus at 70 mm and with dynamic reception focusing (59 frames/s); VI – D&S(D) or delay-and-sum method with both dynamic transmission and reception focusing (the frame rate may be much lower than 59 frames/s).

Para-meter	Depth (mm)	Imaging Method					
		1TX	11TXs	19TXs	91TXs	D&S	D&S(D)
Resolution (mm)	30	1.29	0.93	0.99	0.99	1.02	1.29
	50	2.04	1.29	1.62	1.5	1.68	1.77
	70	2.79	1.68	1.95	2.07	2.37	2.37
	90	3.81	4.05	3.09	2.67	2.97	2.97
Sidelobe (dB)	30	-30.31	-38.4	-41.83	-54.7	-38.29	-52.13
	50	-25.98	-33.66	-37	-46.97	-40.18	-43.44
	70	-23.22	-27.26	-30.32	-40.7	-36.37	-36.37
	90	-19.88	-20.03	-24.68	-34.98	-29.96	-31.18

Table 1. -6dB resolution and average sidelobe (calculated with the average of the left and right 3/8 of each plot that is log compressed) of the point spread functions (PSFs) obtained according to the line plots in Fig. 1.

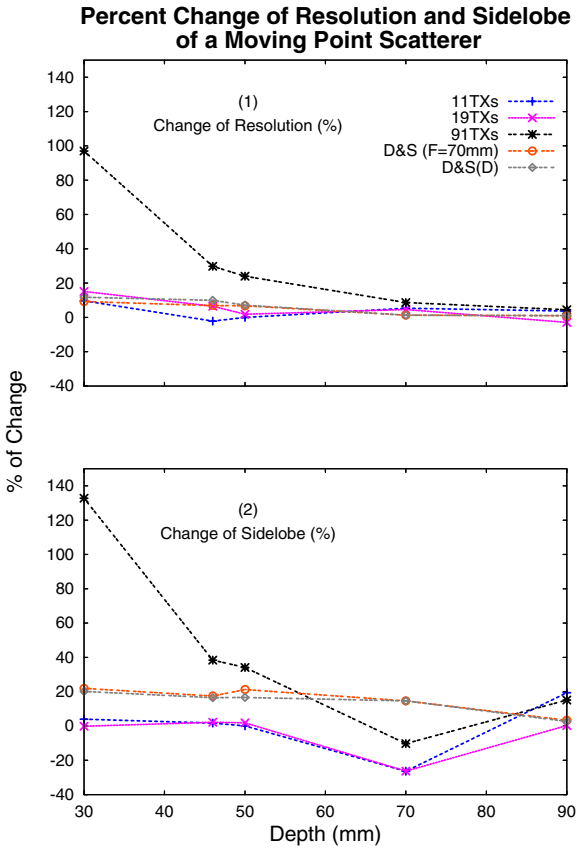

Figure 2. Percent change of (1) resolution and (2) sidelobe of a point scatterer due to its linear motion at a speed of 214 mm/s. The motion is perpendicular to the axial axis of the transducer and is in the imaging plane. The meaning of 11TXs, 19TXs, 91TXs, D&S, and D&S(D) is the same as that of Fig. 1. The percent change is zero for 1TX and thus not shown.

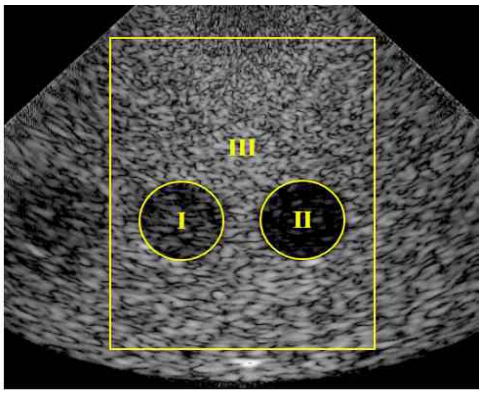

Figure 3. Areas used for the calculation of contrasts of cylindrical objects of an ATS539 tissue-mimicking phantom. The image shown is an example that is obtained with the Fourier method of 91TXs and is log-compressed at 40 dB. In the example, there are two cylindrical objects. A total of 3 such images are used to calculate contrasts of 6 cylindrical objects for each imaging method. Region I is the area that is used to calculate the contrast of one cylinder (the cylinder diameter is 15 mm and the region diameter is 14.1 mm). Region II is the area that has the same size as region I and is used to calculate the contrast of the other cylinder. Region III is a rectangular area excluding both Regions I and II and is used as the background reference for the contrast calculation.

Nominal Contract (dB)	Measured Contrast for Different Imaging Method			
	11TXs	19TXs	91TXs	D&S
-15	-12.31	-14.17	-16.52	-13.70
-6	-7.87	-8.55	-9.07	-7.34
-3	-4.71	-4.54	-4.64	-3.00
+3	2.34	2.34	2.41	4.55
+6	6.05	6.20	6.48	7.55
+15	14.68	14.80	15.09	17.04

Table 2. Contrasts of a stationary ATS539 tissue-mimicking phantom obtained with the *In vitro* experiments. 11TXs, 19TXs, 91TXs, and D&S have the same meaning as those in Fig. 1, except that the focal distance of the D&S method is 46 mm instead of 70 mm. The nominal contrast means the contrast values provided by the manufacturer of the phantom.

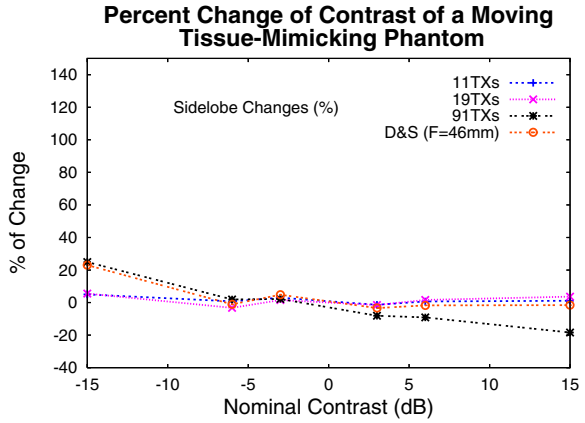

Figure 4. Percent change of image contrast of an ATS539 tissue-mimicking phantom due to its linear motion at a speed of 214 mm/s. The motion is perpendicular to the axial axis of the transducer and is in the imaging plane. 11TXs, 19TXs, 91TXs, and D&S have the same meaning as that in Fig. 1, except that the focal distance of the D&S method is 46 mm instead of 70 mm.

V. Conclusion

The Fourier method developed based on the extended high frame rate imaging theory [7]-[8] is not very sensitive to the motion of object except when the number of transmissions is large (lower frame rate) and the depth is small.

Acknowledgments

The authors would like to thank Mr. Jiqi Cheng for his help in doing the experiments and providing the image construction programs. This work was supported in part by a grant HL 60301 from the National Institute of Health.

References

[1] Jian-yu Lu and J. F. Greenleaf, "Nondiffracting X waves - exact solutions to free-space scalar wave equation and their finite aperture realizations," *IEEE Transactions on Ultrasonics, Ferroelectrics, and Frequency Control*, vol. 39, no. 1, pp. 19-31, January, 1992.

[2] Jian-yu Lu and J. F. Greenleaf, "Experimental verification of nondiffracting X waves," *IEEE Transactions on Ultrasonics, Ferroelectrics, and Frequency Control*, vol. 39, no. 3, pp. 441-446, May, 1992.

[3] Charles Day, "Intense X-shaped pulses of light propagate without spreading in water and other dispersive media," *Physics Today*, v.57, n.10, pp.25-26, October, 2004.

[4] Jian-yu Lu, "2D and 3D high frame rate imaging with limited diffraction beams," *IEEE Transactions on Ultrasonics, Ferroelectrics, and Frequency Control*, vol. 44, no. 4, pp. 839-856, July, 1997.

[5] Jian-yu Lu, "Experimental study of high frame rate imaging with limited diffraction beams," *IEEE Transactions on Ultrasonics, Ferroelectrics, and Frequency Control*, vol. 45, no. 1, pp. 84-97, January, 1998.

[6] Glen Wade, "Human uses of ultrasound: ancient and modern," *Ultrasonics*, vol.38, pp.1-5 (2000).

[7] Jiqi Cheng and Jian-yu Lu, "Fourier based imaging method with steered plane waves and limited-diffraction array beams," in *IEEE 2005 Ultrasonics Symposium Proceedings* (In Press – In the same proceeding as the referring paper).

[8] Jiqi Cheng and Jian-yu Lu, " Extended high frame rate imaging method with limited-diffraction beams," *IEEE Transactions on Ultrasonics, Ferroelectrics, and Frequency Control* (submitted).

[9] Jian-yu Lu, "Limited diffraction array beams," *International Journal of Imaging System and Technology*, vol. 8, no. 1, pp. 126-136, January, 1997 (ISSN: 0899-9457).

[10] R. Bracewell, *The Fourier Transform and its Applications*. New York: McGraw-Hill, 1965, Ch. 4 and 6.

[11] Jian-yu Lu and John L. Waugaman, "Development of a linear power amplifier for high frame rate imaging system," in *IEEE 2004 Ultrasonics Symposium Proceedings*, 04CH37553C, vol. 2, pp. 1413-1416, 2004 (ISSN: 0-7803-8413-X).

[12] Jian-yu Lu, "A multimedia example," *IEEE Transactions on Ultrasonics, Ferroelectrics, and Frequency Control*, vol.50, no. 9, pp. 1078, September, 2003.